The impact of the end-Ordovician glaciation on sediment routing systems: A case study from the Meseta (northern Morocco)

J.-F. Ghienne, A. Benvenuti, M. El Houicha, F. Girard, E. Kali, Y. Khoukhi, C. Langbour, T. Magna, J. Míková, A. Moscariello, et al.

The impact of the end-Ordovician glaciation on sediment routing systems: A case study from the Meseta (northern Morocco)

J.-F. Ghienne[1], A. Benvenuti[2], M. El Houicha[3], F. Girard[4], E. Kali[1], Y. Khoukhi[5], C. Langbour[1], T. Magna[6], J. Míková[6], A. Moscariello[2], K. Schulmann[1,6]

Gondwana Research, 63, 169-178. Doi: 10.1016/j.gr.2018.07.001

[1]Institut de Physique du Globe de Strasbourg, EOST – UMR7516, CNRS/Université de Strasbourg, 1 rue Blessig, F-67084 Strasbourg, France

[2]University of Geneva, 13 rue des Maraîchers, CH-1211, Switzerland

[3]Université Chouaib Doukkali, El Jadida, Morocco

[4]UMR5243, 60 place E. Bataillon, F-34095 Montpellier, France

[5]Université Mohamed I[er], Oujda, Morocco

[6]Czech Geological Survey, Klárov 3, CZ-11821 Prague, Czech Republic

Corresponding author:

Jean-François Ghienne, Institut de Physique du Globe de Strasbourg, EOST – UMR7516, CNRS/Université de Strasbourg, 1 rue Blessig, F-67084 Strasbourg, France

ghienne@unistra.fr

ABSTRACT

Assessment of sediment redistribution by end-Ordovician ice sheets is crucial for the reconstruction of Lower Paleozoic source-to-sink patterns. Focussing on the ice-distal, deepwater Tazekka depocenter (Moroccan Meseta), we thus performed a provenance study that combined whole-rock geochemistry, petrography and insights from high-resolution detrital zircon ages. The results show that the glacigenic sediments are compositionally —mineralogically and geochemically— more mature than preglacial strata. This observation points to a preferential cannibalization of the "great Lower Paleozoic quartz-rich sandstone sheet", with a limited input of first-cycle, far-travelled clastic sediments. Differentiation of glacial units is not straightforward, yet the glaciation acme is typified by a highly mature sedimentary source and an age spectrum lacking Mesoproterozoic zircon grains, both features strongly indicating derivation from the Cambrian–Lower Ordovician cover of the Tuareg Shield. More regional sources are expressed during the earlier glaciation stages, during which lowstand remobilisations unrelated to subglacial erosion are also suspected. Subordinate but notable late Tonian (~ 0.8 Ga) and latest Stenian to early Tonian (~1 Ga) zircon populations are also evidenced in Morocco, which may have implications for future paleogeographic reconstructions.

Keywords

sediment cannibalization, glacial erosion, zircon geochronology, source-to-sink, Hirnantian, peri-Gondwana

1. Introduction

The end-Ordovician glaciation culminated in the growth of a large ice sheet over Gondwana (Le Heron and Craig, 2008; Ghienne et al., 2014; Pohl et al. 2016). From West Africa to Arabia, ice-sheet divides and flow orientations were not necessarily superimposed on preglacial fluvial drainage systems (e.g., Meinhold et al., 2013); the latter serving as guidelines for peri-Gondwana paleotectonic reconstruction based on detrital zircon geochronology (e.g., Pastor-Galán et al., 2013; Shaw et al., 2014). In particular, the assessment of Mesoproterozoic zircon grains in NW Africa is of interest (Avigad et al., 2012; Pratt et al., 2015). As such ages are generally regarded in the north African context as marking a source originating in the Sahara metacraton (NE Africa; Henderson et al., 2015; Chelle-Michou et al., 2017), multi-stage sediment recycling events (see discussion in Andersen et al., 2016) and potential mixing linked to the end-Ordovician glaciation may have severely altered the true significance of zircon provenance. Alternatively, glacially fed routing systems can introduce, or enhance, the contribution of far-travelled sediment sources that were absent or subordinate in preglacial watersheds (Doornbos et al., 2009; Hofmann et al. 2015; Gürsu et al., 2018). For instance, the massive arrival of >2.3 Ga zircon grains that has been detected in the Upper Ordovician strata of the ice-proximal reaches of the glaciated platform in the southern Hoggar (Linnemann et al., 2011) might be a consequence of the reorganization of sediment dispersal trends owing to glaciation. Actually, the degree to which the end-Ordovician glaciation impinged on the Paleozoic dispersal systems of the Gondwana remains unknown (Avigad et al., 2012, 2017).

At the scale of NW Africa, ice flows departing from an oversimplified centrifugal scheme, which in addition does not fully conform to the preglacial fluvial transport directions (Fig. 1), should be supported by changes in sediment provenance preserved

74 in the glacial stratigraphic record. We have performed a systematic and detailed
75 provenance study focusing on the glacigenic sediments of the Tazekka Massif (northern
76 Morocco), a representative area of ice-distal platform segments in end-Ordovician
77 reconstructions (Le Heron et al., 2007). As such, the Tazekka depositional system can be
78 viewed as the final sink of the end-Ordovician, NW African glacial routing system. This
79 new dataset aids in deciphering the impact of the glaciation on the continental-scale
80 sediment dispersal, a resurgence of which may have occurred well after the glacial event
81 through recycling (Pratt et al., 2015). Also, given that the end-Ordovician glaciation
82 corresponds to a polyphase climatic event (Ghienne et al., 2007a, 2014), any clues from
83 high-resolution provenance studies may help to delineate individual advance–retreat
84 cycles of the end-Ordovician ice sheets, provided they relate to distinct sediment routing
85 systems throughout the north-Gondwana platform. We tested if geochronological
86 studies on glacigenic sediments could constitute a valuable tool, which, beyond
87 paleogeographical purposes, could help to better constrain stratigraphic correlations
88 within the end-Ordovician glacial record, e.g. from relatively ice-distal area (Morocco,
89 Europe) toward more internal domains of the north-Gondwana platform (from
90 Mauritania to Chad); such correlations being a pre-requisite for robust paleoclimatic
91 scenarios.
92
93 **2. Geological setting**
94 *2.1. Study area*
95 The Tazekka Massif is a part of the Moroccan Meseta (Fig. 1), the pre-Variscan
96 configuration of which remains unclear, yet generally positioned NW of the Anti-Atlas
97 between the Gondwana landmass and an undefined continental margin (Hoepffner et al.,
98 2005; Michard et al., 2010; Chopin et al., 2014; Pérez-Cáceres et al., 2017). Above a

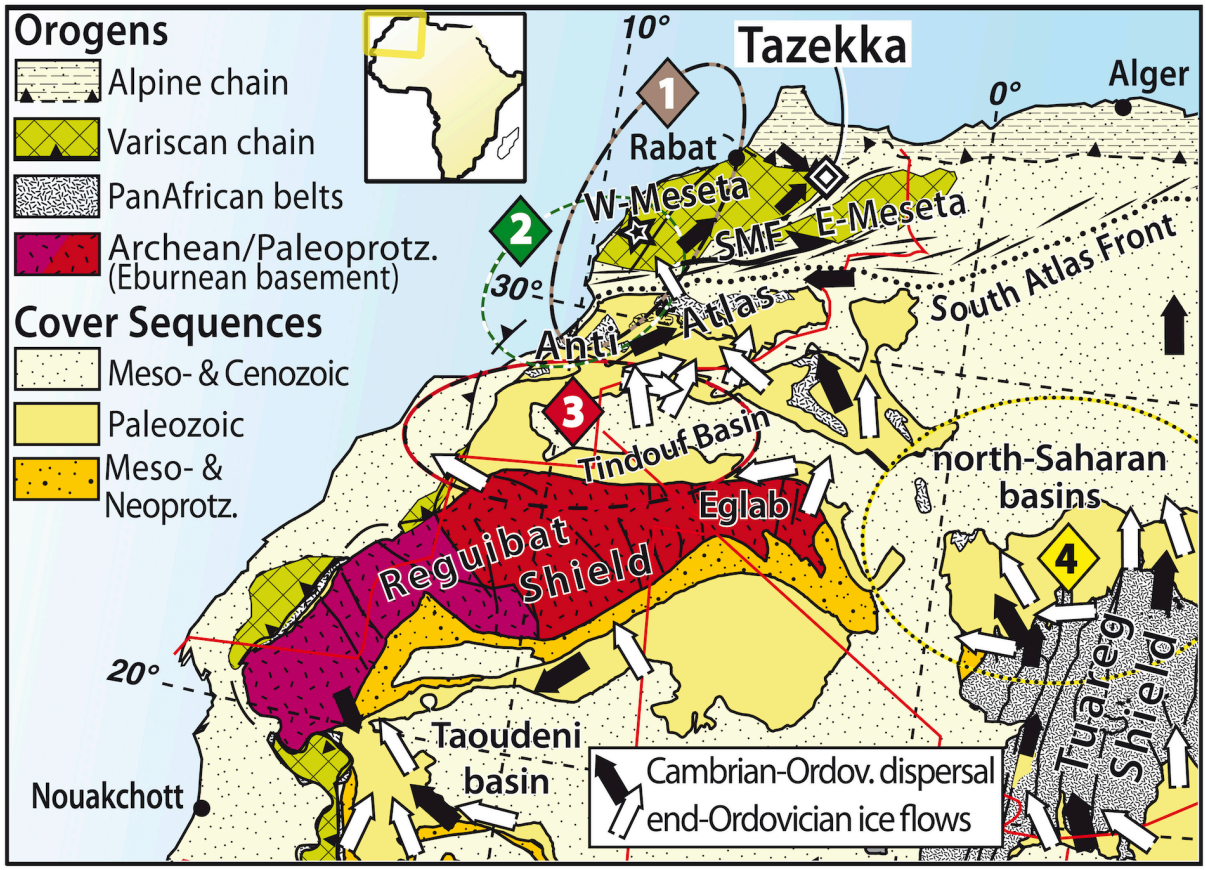

Figure 1. Geological setting (coordinates of the main section in the Tazekka inlier: c. 33,9588°N, 4,3802°W). The Paleozoic configuration was slightly different, owing to poorly constrained Variscan offsets (e.g., along the South Meseta Fault, SMF). The star positions the westernmost Meseta (samples NF01 & 15DL12; Fig. 6). Numbers in diamonds refer to zircon sources (see Figs. 2, 5 and 7). Ice flows orientations mainly from Ghienne et al. (2007), Deschamps et al., (2013), Dietrich et al., in press.

99 preglacial, essentially fine-grained succession (Tehar el Brehl Fm.), there is a thick
100 glacigenic sandstone wedge forming the Tifarouine Fm., which was entirely deposited
101 beyond the end-Ordovician ice fronts (Le Heron et al., 2007, 2008). In the framework of
102 this study, supplementary sections were logged in and around the type area. Our revised
103 stratigraphy allows us to outline five informal stratigraphic members (Fig. 2), the lateral
104 extent of which is in excess of 20 km. Medium-grained sandstones and mudstone
105 interbeds of Mbs 1 and 4 are interpreted as basin-floor turbiditic lobe complexes while
106 amalgamated coarse-grained sandstone sheets of Mbs 3 and 5 represent oversupplied
107 turbiditic systems reflecting two major glacial advances. Glacimarine influence
108 characterizes Mb. 2 (channels, debris-flows, ice-rafted debris), as well as thin interbeds
109 in Mbs 4 and 5. Silurian shales and cherts mark the post-glacial onset of outer shelf
110 conditions. Limited paleocurrent data in turbiditic deposits highlight relatively uniform
111 flows through time from the NW, the W or the SW, yet the original orientations —
112 potentially altered by Variscan thrust tectonics (Hoepffner et al., 2005) — are
113 admittedly unknown.
114
115 *2.2. Paleoglacial setting*
116 From the nearby ice-proximal Anti-Atlas record (Fig. 1), it has been shown that Late
117 Katian and lower Hirnantian lowstand wedges characterize the early glaciation phases,
118 during which glaciers did not reach Morocco (Loi et al. 2010; Ghienne et al., 2014). In
119 contrast, several advance–retreat cycles of the ice sheets are recognized during the late
120 Hirnantian glaciation maximum associated with ice flows from the SE–SSE or from the
121 WNW–WSW (Ghienne et al., 2007a, Le Heron, 2007; Le Heron et al., 2007; Ghienne et al.,
122 2014; Ravier et al., 2015; Dietrich et al., in press). However, temporal correlation of this
123 sequence of events with the Tazekka record is still unresolved.

In Morocco, the glaciers of the end-Ordovician glacial maximum essentially flowed over Upper Ordovician sediments. However, further toward the SW, S or SE, they eroded Lower Ordovician to Cambrian strata (Ghienne et al., 2007 a, b). As shown by rare exotic pebbles —mainly granites, less mafic or metamorphic lithologies— in glacimarine deposits, the basement has directly sourced the glacigenic sediments, at least locally (Fig. 1; Eglab area, Rognon et al., 1972).

3. Methods

3.1. Geochemical and petrographic analysis

Whole-rock geochemical (XRF and LA-ICP-MS) and automated petrographic (QEMSCAN) analysis were performed on seven samples from the Tehar-el-Brehl Fm. and on 36 samples distributed through the five members of the Tifarouine Fm. (19 sandstones, five diamictites and 12 mudstones; Fig. 2). Major element compositions were determined by X-ray fluorescence (XRF) with a *PANalytical Philips PW2400* spectrometer at the University of Lausanne. The trace-element concentrations of whole rocks were measured on glass beads by laser ablation inductively-coupled-plasma mass spectrometry (LA-ICP-MS) with an *Agilent 7700* laser ablation system at the University of Lausanne. Data were reduced with *LAMTRACE* software (Longerich et al. 1996; Jackson 2008). Automated mineral characterization was performed using an *FEI QEMSCAN® Quanta 650F* facility installed at the Department of Earth Sciences, University of Geneva equipped with two *Bruker QUANTAX* light-element energy dispersive X-ray spectrometers at high vacuum, accelerating voltage of 25 kV, and probe current of 10 nA on the carbon-coated polished thin sections. Data processing was performed using the *FEI iDiscover* software package. The effect of weathering, diagenetic, hydraulic sorting, and source rock composition over the compositional

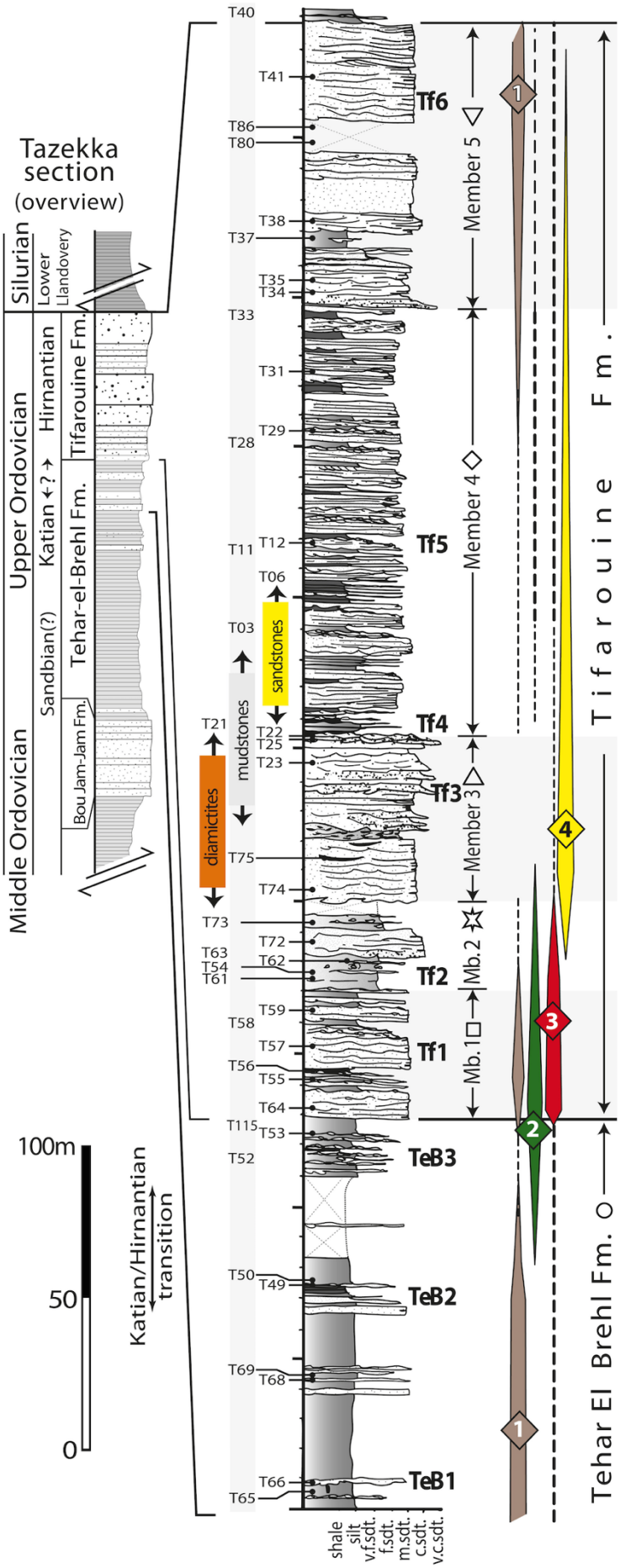

Figure 2. Synthetic section of the Tazekka succession, built from the compilation of five sedimentological logs. On the left, position of samples on which geochemical and petrographic analyses have been performed (Figs. 3 & 4). Samples used for U–Pb geochronology of detrital zircon populations are positioned on the right (TeB 1-3 and Tf 1-6 ; probability plots of Fig. 5). On the right: the inferred scenario for source development (see text for details). Symbols (star, triangle…) associated to stratigraphic units are linked to codes used in figures 3 and 4.

149 results of the investigated samples were investigated following the procedures
150 described in McLennan et al. (1993, 2003), Fralick (2003) and Nesbitt (2003).

151

152 *3.2. U–Th–Pb Geochronology*

153 Three samples from the Tehar el Brehl Fm. (TeB 1-3) and six samples from the
154 Tifarouine Fm. (Tf 1-6) were processed. Detrital zircon grains were separated from
155 several kilograms of samples by sorting, magnetic separation and conventional heavy
156 liquid separation. The final zircon fraction was purified by handpicking in ethanol using
157 a binocular microscope. Zircon samples were mounted in epoxy resin, polished and
158 imaged by cathodoluminiscence to reveal the internal structures of zircon grains by
159 employing a *Tescan* MIRA 3GMU electron microprobe (Oxford Instruments), housed at
160 the Czech Geological Survey.

161 The U–Th–Pb dating was performed using an *Analyte Excite* 193 nm excimer laser
162 ablation system (Teledyne CETAC, Omaha, Nebraska, USA), equipped with a two-volume
163 HelEx ablation cell, in tandem with an *Agilent 7900x* ICPMS (Agilent Technologies Inc.,
164 Santa Clara, USA), housed at the Czech Geological Survey. Samples were ablated in He
165 atmosphere (0.8 l min^{-1}) at a pulse repetition rate of 5 Hz using a spot size of 25 μm and
166 laser fluence of 7.59 J cm^{-2}. Each measurement consisted of 20 s of blank acquisition
167 followed by 40 s sample signal acquisition. The masses 202, 204, 206, 207, 208, 232 and
168 238 were collected using the SEM detector, with one point per mass peak and the
169 respective dwell times of 10, 10, 15, 30, 20, 10 and 15 ms per mass (total sweep time of
170 0.134 s). Instrumental drift was monitored by repeat measurements of 91500 reference
171 zircon (Wiedenbeck et al. 1995) after every 20 unknowns. Data deconvolution using the
172 Iolite software followed the method described by Paton et al. (2010), including an 'on

peak' gas blank subtraction followed by correction for laser-induced elemental fractionation (LIEF) by comparison with the behavior of the 91500 reference zircon (Wiedenbeck et al. 1995). The weighted mean concordia age of 1062.8 ± 2.5 Ma (n = 420, 2σ) was obtained for 91500 reference zircon. In addition zircon reference samples GJ-1 (~609 Ma; Jackson et al. 2004) and Plešovice (337 Ma; Sláma et al. 2008) were analysed periodically during this study and yielded the concordia ages of 607.9 ± 2.8 Ma (n = 170, 2σ) and 338.2 ± 2.3 Ma (n = 320, 2σ), respectively. We have used decay constants incorporated in the Isoplot software (Ludwig, 2012), which are from Jaffey et al. (1971). No common Pb correction has been applied to the data due to the high level of isobaric Hg interferences derived from the carrier gases. We did not apply the $^{207}Pb/^{206}Pb$ criteria for older zircon grains, but the information is included in the data table (Supplementary Material). Instead, the Concordia function of Isoplot software was used for detrital zircon probability plots, which calculates the concordia age based on the $^{206}Pb/^{238}U$ and $^{207}Pb/^{235}U$ ratios and their errors and which yields a more precise mean age than that commonly obtained using either ratio alone.

4. Results

4.1. Insights from petrography and geochemistry

Sandstones share a medium-high compositional maturity while mudstones are relatively enriched in K-rich clay minerals. Glacigenic sandstones are dominated by quartz (>70 modal %, but generally > 80%) and depleted in feldspars; high values of the Chemical Index of Alteration (Nesbitt and Young, 1982) from 65 to 75 and, especially, of the Plagioclase Index of Alteration (> 65 but more usually > 90; Fedo et al. 1995), prove intense weathering in the source area (Fig. 3A). Preglacial sandstones are characterized by higher proportions of detrital sodic feldspars (up to 17 modal %) suggesting less

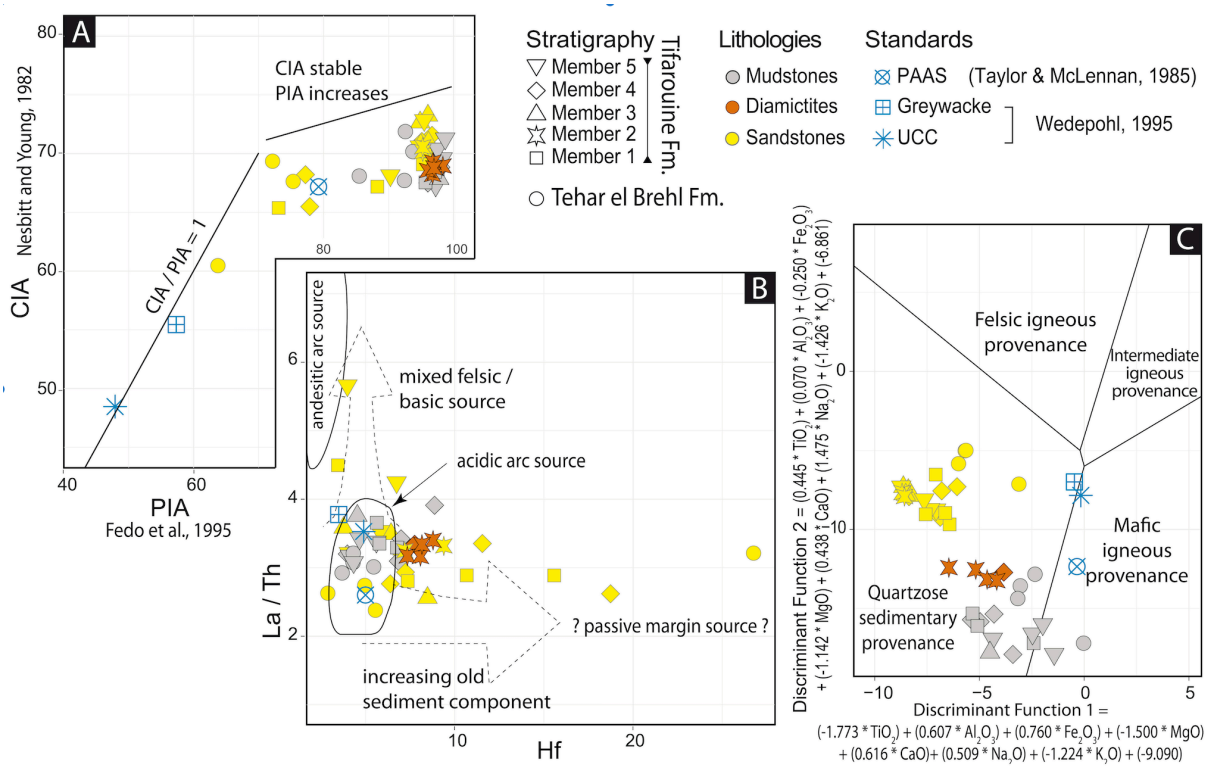

Figure 3. Geochemical results. A: Bivariate diagram between Chemical (CIA, Nesbitt & Young, 1982) and Plagioclase (PIA, Fedo et al., 1995) Indexes of Alteration. B: Provenance characterization diagram (Floyd & Leveridge, 1987). C: Discrimination diagram for sedimentary provenance based on major elements (Roser & Korsch, 1988).

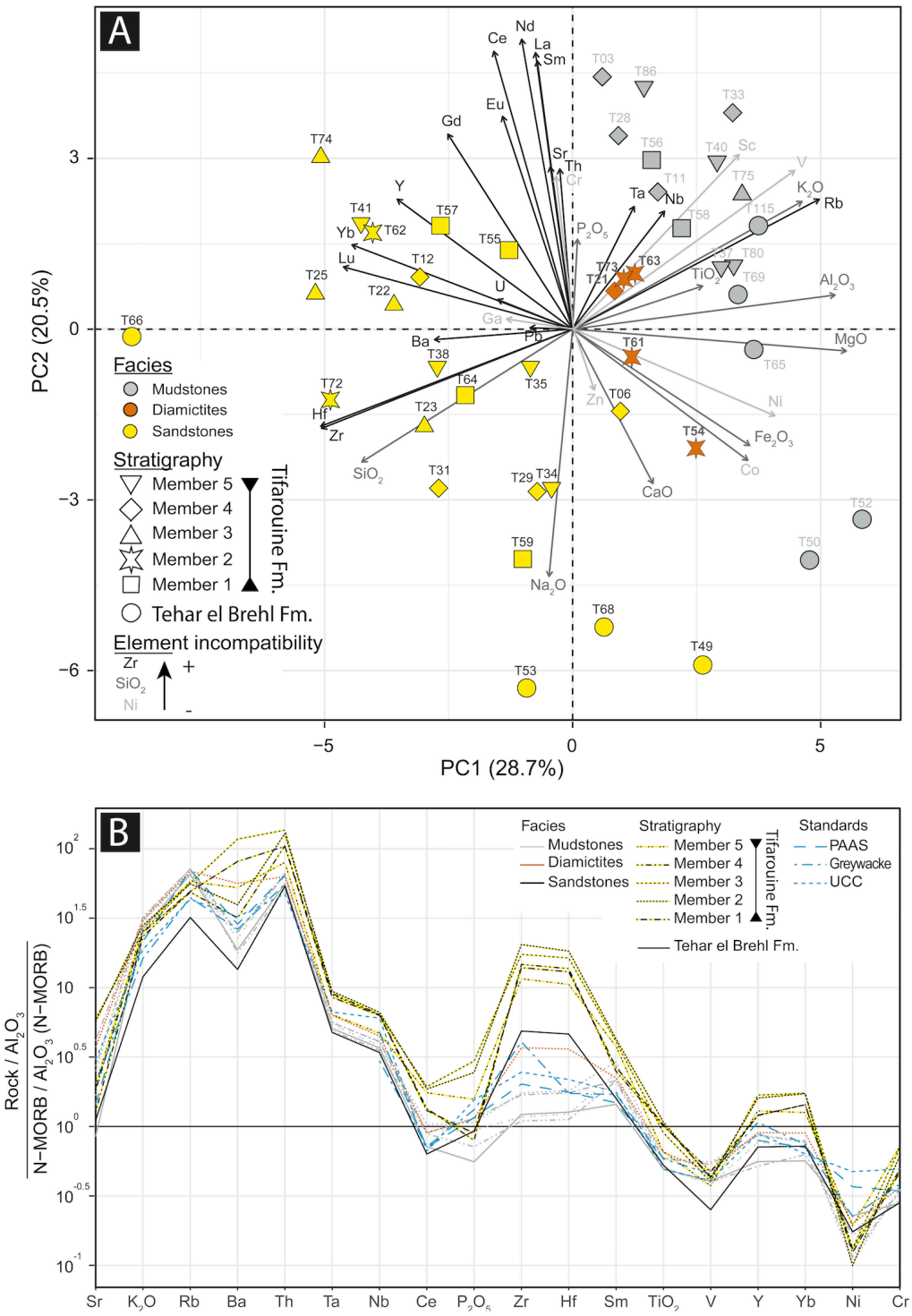

Figure 4. A: Principal component analysis of prevalently immobile elements. The two major components describe roughly half of the total variance of the geochemical composition of the investigated deposits. Na_2O and CaO (largely present in feldspars) and compatible elements correlate positively with the deposits of Tehar-el-Brehl Fm. Incompatible elements correlate with those of the Tifarouine Fm. Mudstones and sandstones are separated along a direction perpendicular to the one that delimits the stratigraphic formations, indicating that grain size does not influence any unit differentiation based on geochemistry. B: Spider diagrams of selected element concentrations of preglacial and glacial deposits normalized to Al_2O_3 and N-MORB. High concentrations of incompatible elements, and LILE (Rb, Cs, Sr, Ba) in particular, compared to the compatible elements suggest that the initial source rock composition of the investigated deposits was acidic.

198 weathered preglacial sources. Notable recycling processes of sedimentary deposits are
199 suggested by the higher-than-average content in sandstones of heavy minerals enriched
200 in Zr–Hf, especially glacigenic sandstones, compared to the greywacke and UCC standard
201 values (Fig. 4B). The greater maturity of the glacigenic sediments, for which a higher
202 degree of chemical alteration is unlikely (Bahlburg and Dobrzinski 2011), highlights a
203 re-organization in sediment provenance at the glaciation onset. A discriminant diagram
204 based on major elements (Roser and Korsch, 1988) confirms that a sedimentary source
205 was prevalent (Fig 3C). The compositional difference between the Tehar-el-Brehl and
206 Tifarouine Fms. must be principally related to distinct composition of the sedimentary
207 sources. This is in line with a principal component analysis of major and trace elements
208 concentrations (Fig. 4A) showing preferential enrichment of incompatible elements in
209 glacigenic deposits, which suggests that the source rocks of the glacigenic sediments
210 were originally derived from more evolved magmatic rocks.
211 Glacigenic sediments mutually differ very slightly, with the exception of higher
212 concentrations of elements such as Hf in individual sandstone samples of Mbs 1 & 4 (Fig.
213 3B). Interestingly, abundance shifts are not reflected by a higher maturity of those
214 samples and are recorded in both sandstones and mudstones. This indicates a
215 preferential reworking of strata that were already enriched in heavy minerals (zircon,
216 monazite), for instance coastal placers, which are recurrently observed in Ordovician
217 nearshore deposits (e.g., Pistis et al., 2016). Diamictites are plotted in between
218 sandstones and mudstones (Figs. 3C and 4A), indicating grain-size mixing rather than a
219 specific sourcing. Sandstones in Mbs 2 and 3 are associated with the most
220 mineralogically and geochemically mature source composition. This is particularly
221 apparent in Figs. 3A, 3C and 4B where these sandstones have, for instance, and on
222 average, (i) higher indices of alteration, (ii) parameters indicative of a sedimentary

source largely dominated by a quartzose provenance, and (iii) higher concentrations of P_2O_5, Hf, Zr, Yb. This does not solely reflect the coarse-grained nature of the deposits as samples of the similarly coarse-grained Mb. 5 behave distinctively. The more mafic composition of the latter marks the resumption of a preglacial signal, which was never totally cut off during the glaciation as shown by some specific samples in Mbs 1 & 4, the composition of which echoes the one of the preglacial deposits.

4.2. Insights from U–Th–Pb datings

The U–Th–Pb LA-ICPMS measurements were performed on 881 detrital zircon grains from the nine samples of the Tazekka section. Probability plots in Fig. 5 only include ages with a concordance between 95 and 105%. One additional probability plot from the glacigenic sediments of the westernmost Meseta (NF01) is also given (Fig. 6B), to compare with the ages from a middle–upper Cambrian sandstone of the same area (15DL12; Letsch et al., 2018; Fig. 6B). The compilation of the 881 ages of the Tazekka section (Fig. 6C) shows a very similar age distributions for the 50–100µm and 100–250 µm grain-size ranges, which indicates that hydraulic processes did not significantly impact our zircon record.

It is apparent from Figs. 5 and 6C that Cryogenian–Ediacaran (Pan-African, 580–720 Ma; Ennih and Liégeois, 2001; Gasquet et al., 2008) and Paleoproterozoic (Eburnean, 1790–2300 Ma, Abati et al., 2012) ages dominate the record. The two populations, and the lull in between, which corresponds to the West African magmatic gap of Linnemann et al. (2011), are regarded as a signature of the western segment of the north Gondwana platform. Except sample Tf 3 showing the greatest ratio of Pan-African to Eburnean zircon grains (59 vs. 24%), which is comparable to most of previous published works (Linnemann et al., 2011; Avigad et al., 2012; Gärtner et al., 2017), the

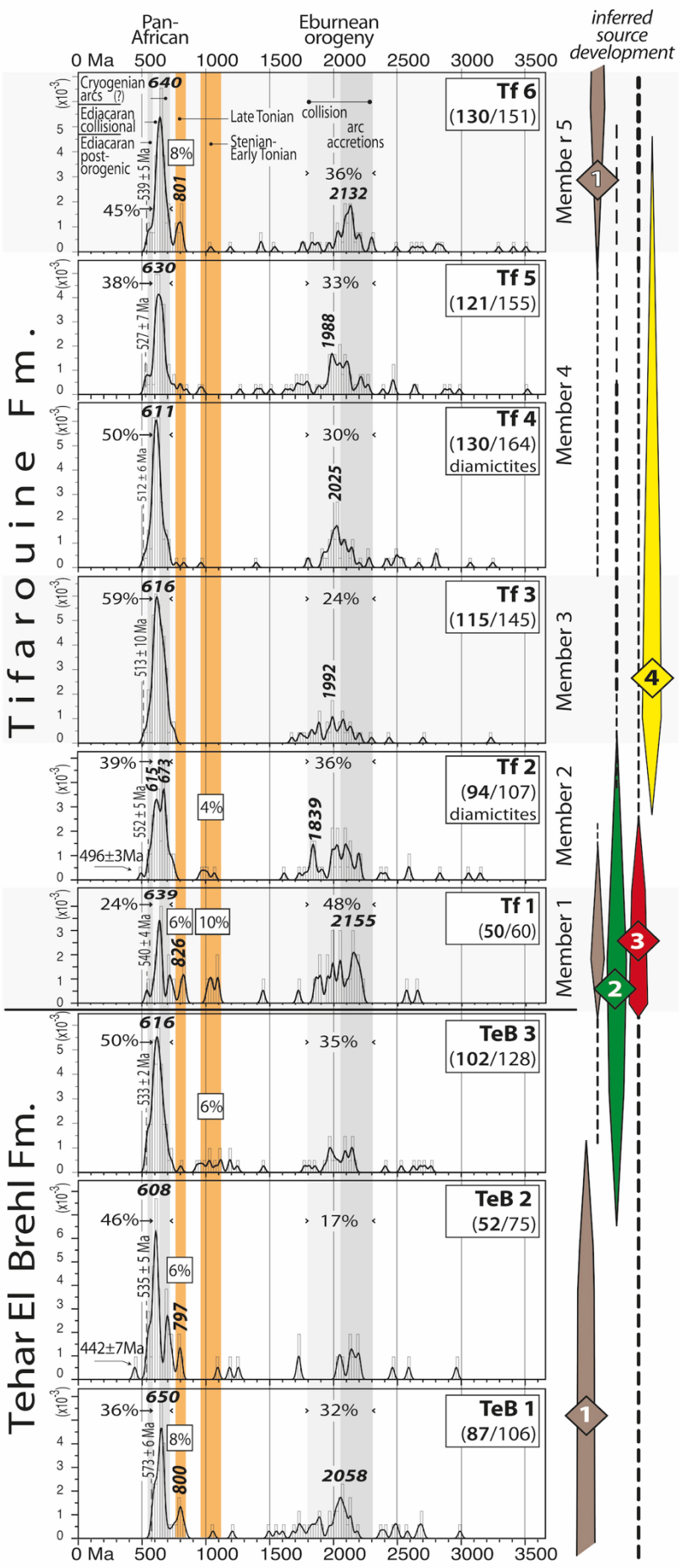

Figure 5. Binned frequency (bin size: 20 Ma) and probability density distribution plots of concordant zircon ages from the end-Ordovician Tazekka record. Late Tonian and late Stenian–early Tonian populations (orange bands) are particularly well defined in TeB 2 and Tf 1, in spite of a limited number of measured ages. Minimum zircon ages are specified on the left of each plot as well as proportion (%) of distinctive populations. Note that the scenario for source development also integrates petrographic and geochemical insights (section 4.1. and Fig. 2).

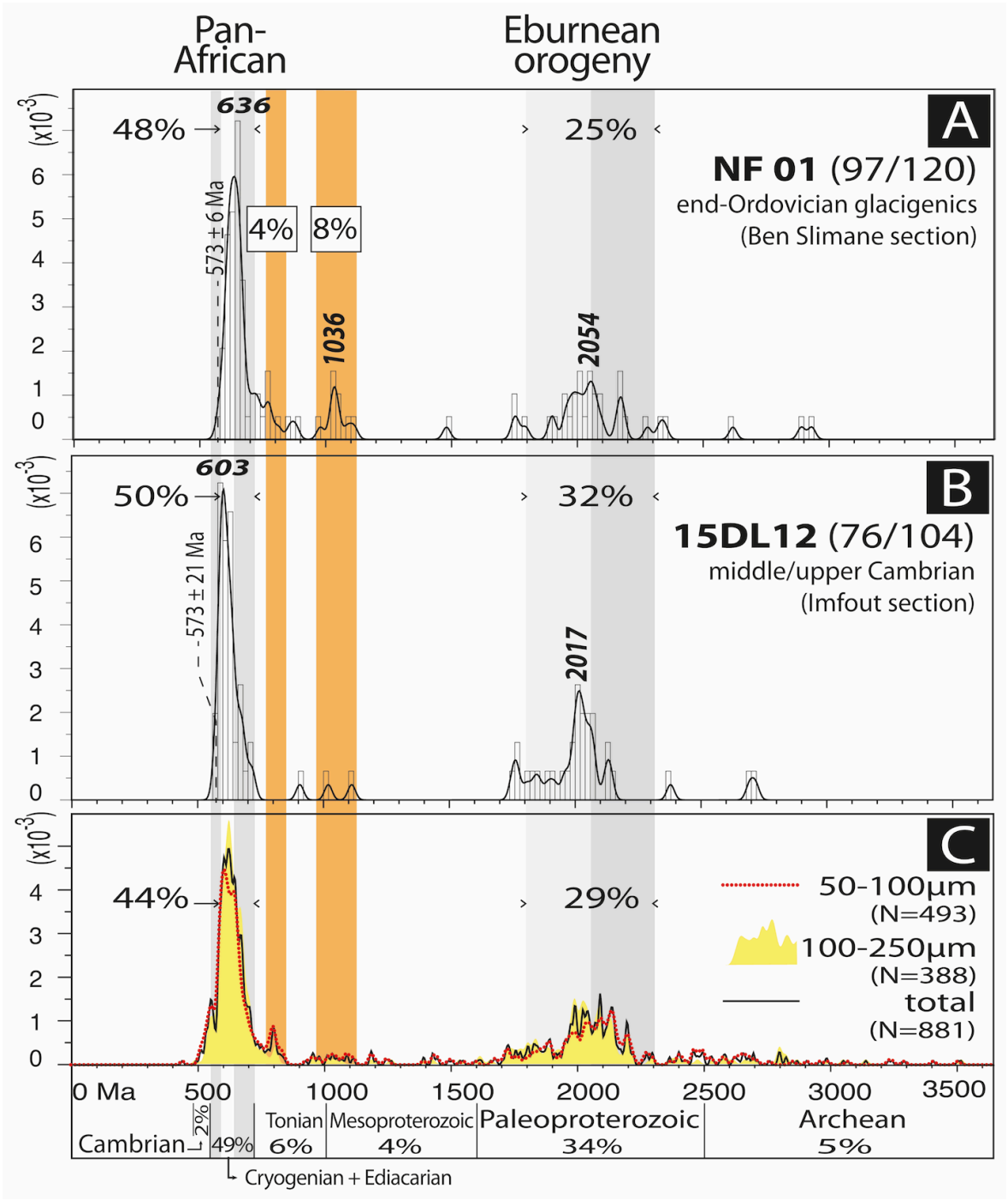

Figure 6. A & B: Binned frequency (bin size: 20 Ma) and probability density distribution plots of concordant zircon ages from samples of the westernmost Meseta ('Coastal Block', located by the black star in Fig. 1), either (A) glacigenic deposits of the Ben Slimane section (this study) or (B) middle-upper Cambrian strata, El Hank Fm., Imfout section (modified from Letsch et al., 2018). C: age compilation of the 881 zircon ages of the Tazekka section plotted in Fig. 5. Orange bands refer to the late Tonian and late Stenian–early Tonian population discussed in the text. Grey bands in Pan-African ages, see Fig. 5.

other glacigenic samples have a notable proportion of Eburnean zircon grains and sample Tf 1 yields significantly more Eburnean (48%) than Pan-African (24%) zircon grains.

Several Archean and Cambrian zircon grains were also detected, the latter being absent from the westernmost Meseta (Fig. 6). Post-orogenic Late Ediacaran zircon grains form a restricted population (<8%), which peaks at 554Ma (Fig. 6C), yet it is most often identifiable in the form of a shoulder rather than an actual peak in individual plots (Fig. 5). Most interesting are two subordinate but distinctive populations: a late Tonian population, ranging from 840 to 760 Ma, and a late Stenian–early Tonian population showing a broader age cluster, ca. 960–1120 Ma (~1 Ga; Fig. 5). The latter, best observed in sample Tf 1, is also well defined in NF01. These two age populations, though their presence/absence characterizes and differentiates some samples in this study (Fig. 5), appear poorly detectable in the age compilation (Fig. 6C).

5. Discussion

5.1. Deciphering sediment sources.

The fact that the westernmost Meseta zircon record is similar to that of the deeper-water Tazekka succession is in line with the northeastward (±45°) orientation of shelf progradation across the Meseta during the Ordovician (Razin et al., 2002). However, latest Ediacaran–early Cambrian zircon grains throughout the Tifarouine Fm., absent from NF01 and 15DL12, suggest that the Tazekka watershed was not restricted to the Meseta. This is corroborated by the great thickness of the glacigenic succession (>350 m), largely exceeding that of other coeval peri-Gondwanan records that are generally no more than a few tens of metres in thickness (Chatalov, 2017 and references therein). The Tazekka was connected to the West African dispersal system and its relatively

273 isolated current location at the NE tip of Western Meseta (Michard et al., 2010) cannot
274 be fully representative of the Lower Paleozoic configuration.
275 The overall Tazekka record combining sedimentology, geochemistry and insights
276 from zircon populations is best understood in terms of the interplay of four sources that
277 can be inferred for the Ordovician in and around Morocco (Figs. 2 and 5). Preglacial
278 Source 1 has a less mature composition and includes the late Tonian zircon population
279 (TeB 1 and TeB 2). Sample TeB 3 shows the cut-off of Source 1 or, more probably, its
280 dilution by Source 2, which is marked by the ~1 Ga zircon population. Associated with
281 the onset of sandstone deposition in the uppermost preglacial sediments, Source 2 also
282 characterizes the glacigenic deposits of the westernmost Meseta (Fig. 6). Source 3 is
283 inferred from the Tf 1 and Tf 2 record, typified by a great proportion of Eburnean zircon
284 grains. In Mb 1, at the base of the Tifarouine Fm., the late Tonian (i.e. 840–760 Ma) and
285 ~1 Ga populations are well defined, suggesting that sources 1 and 2 were still active,
286 either directly, or indirectly through the reworking of older strata. Source 4 (Tf 3) shows
287 the most mature composition (Mb. 3 in Figs 3 and 4), the greatest Pan-African zircon
288 grains, the younger Cambrian zircon population, a striking West African magmatic gap
289 — no more Mesoproterozoic zircon grains in discordant ages — and no Tonian zircon
290 grains. The overlying glacimarine interbed (Tf 4) mainly shares similar features. Due to
291 its association with the coarsest unit (Mb. 3), Source 4 is regarded as linked to the
292 maximum advance of the end-Ordovician glaciers in NW Africa. It may have been
293 activated slightly earlier in the succession, considering that the compositional signature
294 of the sandstone filling in the channels of the glaciomarine depositional system (Mb. 2)
295 is similar to that of Mb. 3 (see above; Figs. 3C & 4B). In the upper part of the Tifarouine
296 Fm., samples Tf 5 and Tf 6 show the re-appearence of Mesoproterozoic zircon grains and
297 the progressive re-increase of the Eburnean zircon population. Further, a recurrence of

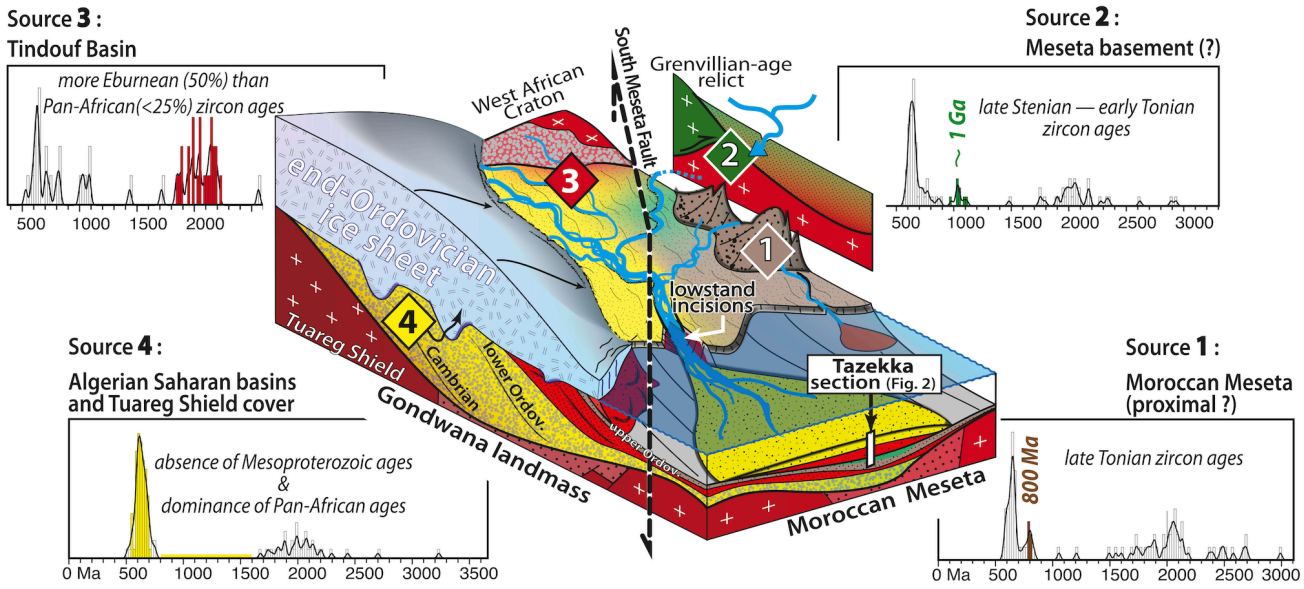

Figure 7. Conceptual model for glaciation-impacted sediment dispersal trends as understood from the Tazekka record. Patterns and colours as in Fig. 1. Numbers in diamonds relate to provenances discussed in the text (see also Fig. 2), the proposed location of which is given in Fig. 1. Probability plots selected from Figs. 5 and 6 illustrate the zircon age records tied to individual sources that together mixed and fed the Tazekka depocenter. Source 4 originates from glacial erosion of the Cambrian-Ordovician sedimentary cover (Algerian basins, Tuareg Shield cover), while other sources, of more local origin, may have involved a significant contribution of lowstand cannibalisations (fluvial incisions, shelf-margin canyons) and restricted truly glacigenic inputs.

298 the late Tonian population is recognized in Tf 6 (Fig. 5). It reflects the progressive
299 upwards dilution of Source 4 understood as a recovery stage after the glaciation
300 maximum. This is in line with slightly more mafic compositions noted in Mb. 5 samples,
301 a reminiscence of a signal observed in preglacial samples of the Tehar el Brehl Fm. (Fig.
302 3C). The last glacial advance, marked by renewed coarse-grained sedimentation in Mb.
303 5, remobilized a material dominated by Source 1. As sediment sources are suspected to
304 continuously mix through time, none of the probability plots (Figs 5 and 6) is so far fully
305 representative of one particular provenance. Four of them, which can be regarded as
306 typifying each of the four proposed provenances, are however used in Figure 7 to
307 approximate, or at least illustrate, the zircon age records tied to individual sources that
308 together fed the Tazekka depocenter.
309
310 *5.2. Sediment sources and glaciation development*
311 The scenario of sediment source development through the Tazekka stratigraphic
312 record, representing only a ca. 5 Myr time span, is understood in the framework of the
313 end-Ordovician glaciation. In addition, the regional-scale source diversity arisen from
314 the complex Lower Paleozoic evolution around the Meseta domain during peri-
315 Gondwana rifting events should be considered. Source 1 in preglacial sediments shows a
316 contribution of first-cycle clastic sediments, potentially in relation with a single Upper
317 Ordovician zircon recovered in TeB 2. We suspect a genetic link with a coeval thermal
318 event (Clauer et al., 1995) and the local denudation of Ediacaran basement rocks (Tahiri
319 et al., 2010) (Fig. 7), both possibly related to the magmatic (e.g., Caroff et al., 2009)
320 and/or extensional events (e.g., Martinez-Catalan et al., 1992) affecting the north-
321 Gondwana domain at the end of the Ordovician. The late Tonian population, which is
322 absent from sample 15DL12 from Cambrian strata of Coastal Meseta (Letsch et al., 2018;

Fig. 6), reflects the erosion of rocks exposed only after the Cambrian, which are possibly in relation with uplifts tied to the opening of Rheic ocean (Ouanaimi et al., 2016; Gärtner et al., 2017). The paucity of Cambrian zircon grains indicates that (i) Cambrian rift basins (Pouclet et al., 2008; Michard et al., 2010; Letsch et al., 2018) were buried at that time, and (ii) the Eburnean basement of the Meseta cannot be considered as a source for Paleoproterozoic zircon ages (e.g., El Houicha et al., 2018).

Source 2, activated prior to the onset of massive sandstone deposition in the Tazekka, and relatively well-defined in the westernmost Meseta (Fig. 6A), suggests that the ~1 Ga zircon population reflects the activation of a nearby source. Indeed, ~1 Ga zircon grains do not represent contribution of a more southern remote source, which would have had a wider age spectrum regarding Mesoproterozoic ages (De Waele et al., 2015; Gärtner et al., 2017). Combined with other ~1 Ga ages documented in the Moroccan context (a charnockite outcrop off Morocco, Michard et al., 2010; recycled zircon in Ediacarian granites, Tahiri et al., 2010; recycled zircon in Trias volcanics, Marzoli et al., 2017), Source 2 highlights the existence a currently undefined relict of Grenvillian-aged crust. The latter has sourced, most likely from the west, directly (erosion of Mesoproterozoic rocks) or indirectly (erosion of late Neoproterozoic magmatic rocks having recycled Mesoproterozoic zircon), the end-Ordovician Moroccan glacial dispersal system (Fig. 7), independently from other well-known sources related to the largely more eastern Saharan metacraton (e.g., Meinhold et al., 2013; Henderson et al., 2015). This ca. 1 Ga zircon population may derived from an exotic terrane issuing from an Avalonian crust and later accreted, during the Pan-African and/or Cadomian developments, to the West African Craton (Abbo et al., 2015; Marzoli et al., 2017; Gärtner et al., 2017). The ca. 1 Ga zircon population, predating the massive arrival of

glacigenic sediments, is not introduced in the Moroccan context by the end-Ordovician glaciation (see discussion in Pratt et al., 2015).

Source 3 is tied to the onset of mature glaciation-related deposits (Mb. 1), yet it was continuously providing sediments as shown by the great proportion of Eburnean zircon grains in the overall Tazekka record (Fig. 6C). In Mb. 1 of the glacigenic Tifarouine Fm., both the high Hf content that reflects the reworking of coastal placers, and the lack of evidence for any glacial depositional processes, suggest the local remobilisation of an older shelf succession; the later yielding a prevalent Eburnean population. The Source 3 signal is absent, or at least subordinate, in the westernmost Meseta (Fig. 6). It points to a southern derivation of material tied to the recycling of Cambrian–Ordovician strata of the Tindouf Basin, which themselves have been initially sourced predominantly from an Eburnean basement (Reguibat Shield; Fabre and Kazi-Tani, 2005; Fig. 1). Whether or not the Sources 2 and 3 have involved glacial erosions remains unclear. Additional work is needed to decipher if this sequence is related to watershed reorganisations, including meltwater captures and then glacigenic sediments, or to strictly localized lowstand cannibalizations (e.g., incised valley or shelf-margin canyon; Fig. 7).

Showing none of the local signals, glacial maximum strata (Mb. 3 of the Tifarouine Fm.) were principally fed from outside the Meseta and are tied to a fourth provenance. Source 4 provides evidence for a major remobilization of the Cambrian–Ordovician strata from the northern Saharan Basins or of the ancient cover of the Tuareg Shield (Fabre and Kazi-Tani, 2005), the age spectrum of which (Linnemann et al., 2011) is very similar to sample Tf 3. Source 4 is thus viewed as the signature of the NW-oriented ice flows recognized in the Anti-Atlas (Fig. 1), and originating from the surroundings of the current Tuareg Shield, where glacial downcuttings essentially eroded the Cambrian-Ordovician cover, and more rarely the Pan-African rocks of the Trans-Saharan Belt (Fig.

7; Fekirine and Abdallah, 1998; Ghienne et al., 2007b; Deschamps et al., 2013). The flux of >2.3 Ga zircon grains detected upstreamward (Linnemann et al., 2011), which is unrecognized in the Tazekka sequence, is suspected to correspond to a local and transient input, rapidly redistributed by postglacial transgressive systems (cf. HOG6 and HOG7 probability plots of Linnemann et al., 2011). Coarse-grained sediments of Mb. 5, compositionally slightly less mature and showing a renewed contribution of Source 1, suggest that the last glacial advance reworked a great proportion of local material, most likely including earlier end-Ordovician glacigenics, with a fading contribution of Source 4. Mb. 5 is tentatively linked with glaciers that, in the Anti-Atlas, flowed from the W (Dietrich et al., in press).

6. Conclusions

The Tazekka glacigenic deposits essentially derived from the cannibalization of the "great Lower Paleozoic quartz-rich sandstone sheet", itself initially having recycled the Pan-African molasse and flysch basins (Avigad et al., 2017), rather than recording a pulse of fresh, far-travelled, first-cycle clastic sediments issuing from basement rocks. This finding is in line with conclusions of Chatalov (2017) and Gärtner et al. (2017), also dealing with the north Gondwana area but is in contrast with common views about the limited maturity of syn-glaciation deposits (Nesbitt and Young, 1982; Yan et al., 2010; Bahlburg and Dobrzinski, 2011; Huang et al. 2014). More interestingly, end-Ordovician glacigenic deposits in South Africa show a significantly lower CIA than that of the underlying preglacial succession (Young et al., 2004), which is in contrast to the north-Gondwanan examples from this study, even regarding the diamictite samples (Fig. 3A). It might suggest two distinct modes of glacial erosion, involving eroding highlands in the

first case, essentially recycling the preglacial shelf sediments in the second case, with potential contributions from remote highlands absent or greatly diluted.

Glacial erosion of the Cambrian–Ordovician strata, especially during the glacial maximum, boosted the transfer of compositionally —i.e., mineralogically and geochemically— mature material toward the continental margin, temporarily masking regional signals expressed only before the glaciation or in its earlier stages (late Tonian and late Stenian–early Tonian zircon ages, respectively). The glacial maximum was responsible for a notable provenance change of a broader significance which may be traceable outside Morocco, rather than just be a result of local adjustments. The first-order, continental-scale Lower Paleozoic dispersal trends nevertheless pertained through the glaciation. They were buffered by the voluminous, north-African Lower Paleozoic sandstones that furnished the main contribution to the glacigenic material, which consequently show more mature compositions than those prevailing in Morocco prior to the end-Ordovician glaciation.

ACKNOWLEDGEMENTS

The authors are thankful to Dov Avigad, N. Eyles and an anonymous reviewer, whose comments greatly contributed to the improvement of the original manuscript. This work is a contribution to the SeqStrat-Ice ANR project 12-BS06-14. It was partly funded by the joined industry project GRASP (University of Geneva), the Fondation Lombard (Geneva), and the Czech Ministry of Education, Youth and Sports (project LK11202). We are grateful to Patricie Halodová for help with cathodoluminiscence imaging.

421 **REFERENCES**

422 Abati, J., Aghzer, A.M., Gerdes, A., and Ennih, N., 2012. Insights on the crustal evolution of
423 the West African Craton from Hf isotopes in detrital zircons from the Anti-Atlas belt.
424 Precambrian Research 212-213, 263–274.

425 Abbo, A., Avigad, D., Gerdes, A. and Güngör, T., 2015. Cadomina basement and Paleozoic
426 to Triassic siliciclastics of the Taurides (Karacahisar dome, south-central Turkey):
427 Paleogeographic constraints from U-Pb-Hf in zircons. Lithos 227, 122–139.

428 Andersen, T., Kristoffersen, M., and Elburg, M.A., 2016. How far can we trust provenance
429 and crustal evolution information from detrital zircons? A South African case study.
430 Gondwana Research 34, 129–148.

431 Avigad, D., Gerdes, A., Morag, N., and Bechstädt, T., 2012. Coupled U–Pb–Hf of detrital
432 zircons of Cambrian sandstones from Morocco and Sardinia: Implications for
433 provenance and Precambrian crustal evolution of North Africa. Gondwana Research,
434 21, 690–703.

435 Avigad, D., Morag, N., Abbo, A., and Gerdes, A., 2017. Detrital rutile U-Pb perspective on
436 the origin of the great Cambro-Ordovician sandstone of North Gondwana and its
437 linkage to orogeny. Gondwana Research 51, 17–29.

438 Bahlburg, H., and Dobrzinski, N., 2011. A review of the Chemical Index of Alteration
439 (CIA) and its application to the study of Neoproterozoic glacial deposits and climate
440 transitions. In: Arnaud, E. et al. (Eds.), The Geological Record of Neoproterozoic
441 Glaciations, pp. 81-92 Geological Society London, Memoirs.

442 Caroff, M., Vidal, M., Bénard, A., and Darboux, J.-R., 2009. A late-Ordovician
443 phreatomagmatic complex in marine soft-substrate environment: The Crozon

444 volcanic system, Armorican Massif (France). Journal of Volcanology and Geothermal
445 Research 184, 351–366.

446 Chatalov, A., 2017. Sedimentology of Hirnantian glaciomarine deposits in the Balkan
447 Terrane, western Bulgaria: Fixing a piece of the north periGondwana jigsaw puzzle.
448 Sedimentary Geology 350, 1–22.

449 Chelle-Michou, C., Laurent, O., Moyen, J.-F., Block, S., Paquette, J.-L., Couzinié, S., Gardien,
450 V., Vanderhaeghe, O., Villaros, A., and Zeh, A., 2017. Pre-Cadomian to late-Variscan
451 odyssey of the eastern Massif Central, France: Formation of the West European crust
452 in a nutshell. Gondwana Research 46, 170–190.

453 Chopin, F., Corsini, M., Schulmann, K., El Houicha, M., Ghienne, J.-F. and Edel, J.-B., 2014.
454 Tectonic evolution of the Rehamna metamorphic dome (Morocco) in the context of
455 the Alleghanian-Variscan orogeny. Tectonics 33, 1154–1177.

456 Clauer, N., Rais, N., Schaltegger, U., and Piqué, A., 1995. K–Ar systematics of clay-to-mica
457 minerals in a multi-stage low-grade metamorphic evolution. Chemical Geology 124,
458 305–316.

459 Deschamps, R., Eschard, R., and Roussé, S., 2013. Architecture of Late Ordovician glacial
460 valleys in the Tassili N'Ajjer area (Algeria). Sedimentary Geology 289, 124–147.

461 De Waele, B., Lacorde, M., Vergara, F., and Chan, G., 2015. New insights on Proterozoic
462 tectonics and sedimentation along the peri-Gondwanan West African margin based
463 on zircon U–Pb SHRIMP geochronology. Precambrian Research 259, 156–175.

464 Dietrich, P., Ghienne, J.-F., Lajeunesse, P., Deschamps, R., Normandeau, A., Razin, P., in
465 press. Deglacial sequences and glacio-isostatic adjustment. Quaternary compared
466 with Ordovician glaciations. In: Glaciated Margins: The Sedimentary and Geophysical
467 Archives, D. Le Heron et al. (Eds), Geological Society London, Spec. Publ. 475.

468 Doornbos, C., Heaman, L.M., Doupé, J.P. , England, J., Simonetti, A., and Lajeunesse, P.,
469 2009. The first integrated use of in situ U–Pb geochronology and geochemical
470 analyses to determine long-distance transport of glacial erratics from mainland
471 Canada into the western Arctic Archipelago. Canadian Journal of Earth Science 46,
472 101–122.

473 El Houicha, M., Peirera, M.F., Jouhari, A., Gama, C., Ennih, N., Fekkak, A., Ezzouhairi, H., El
474 Attari, A., and Silva, J.B., 2018. Recycling of the Proterozoic crystalline basement in the
475 Coastal Block (Moroccan Meseta): New insights for understanding the geodynamic
476 evolution of the northern peri-Gondwanan realm. Precambrian Research 306, 129–
477 154.

478 Fabre, J., and Kazi-Tani, N. 2005. Ordovicien, Silurien, Devonien, Permo-Carbonifère,
479 147-360. In : Fabre, J. (Ed.) Géologie du Sahara occidental et central, Tervuren African
480 Geoscience Collection 18, Musée Royal de l'Afrique Centrale, Tervuren, Belgium.

481 Fedo, C. M., Nesbitt, H. W., and Young, G. M., 1995. Unraveling the effects of potassium
482 metasomatism in sedimentary rocks and paleosols, with implications for
483 paleoweathering conditions and provenance. Geology 23, 921–924.

484 Fekirine, B., and Abdallah, H., 1998. Palaeozoic lithofacies correlatives and sequence
485 Stratigraphy of the Sahara Platform, Algeria. In: Maccregor, D.S., Moody, R.T.J., Clark-
486 Lowes, D.D. (Eds.) ,Petroleum Geology of North Africa. Pp. 97–108. Geological Society
487 London Special Publication 132.

488 Floyd, P.A., and Leveridge, B.E., 1987. Tectonic environment of the Devonian Gramscatho
489 bason, south Cornwall : Framework mode and geochemical evidence from turbiditic
490 sandstones. Journal of the Geological Society 144, 531–542.

491 Fralick, P. W., 2003. Geochemistry of clastic sedimentary rocks: ratio techniques. In:
492 Lentz, D. R. (Ed.): Geochemistry of Sediments and Sedimentary Rocks: Evolutionary
493 Considerations to Mineral Deposit-Fanning Environments. Geological Association of
494 Canada, GeoTexl 4.

495 Gärtner, A., Youbi, N., Villeneuve, M., Sagawe, A., Hofmann, M., Mahmoudi, A., Boumehdi,
496 M.A., and Linnemann, U., 2017. The zircon evidence of temporally changing sediment
497 transport—the NW Gondwana margin during Cambrian to Devonian time (Aoucert
498 and Smara areas, Moroccan Sahara). International Journal of Earth Sciences 106,
499 2747-2769.

500 Gasquet, D., Ennih, N., Liegeois, J. P., and Michard, A., 2008. The Pan-African Belt.
501 Continental evolution. The geology of Morocco: Structure, Stratigraphy, and Tectonics
502 of the Africa-Atlantic-Mediterranean Triple Junction, pp. 33-64 Springer Verlag
503 Berlin, Heidelberg.

504 Ghienne, J.-F., Le Heron, D., Moreau, J., Denis, M., and Deynoux, M. 2007a. The Late
505 Ordovician glacial sedimentary system of the North Gondwana platform. In: Hambrey,
506 M., Christoffersen, P., Glasser, N., Janssen, P., Hubbard, B., Siegert, M (Eds.), Glacial
507 Sedimentary Processes and Products. pp. 295–319 Internal Association of
508 Sedimentologists, Special Publication 39.

509 Ghienne, J.-F., Boumendjel, K., Paris, F., Videt, B., Racheboeuf, P., and Salem, H.A., 2007b.
510 The Cambrian-Ordovician succession in the Ougarta Range (western Algeria, North
511 Africa) and interference of the Late Ordovician glaciation on the development of the
512 Lower Palaeozoic transgression on northern Gondwana. Bulletin of Geosciences 82,
513 183–214.

514 Ghienne, J.-F., Desrochers, A., Vandenbroucke, T.R.A., Achab, A., Asselin, E., Dabard, M.-
515 P.,Farley, C., Loi, A., Paris, F., Wickson, S., and Veizer, J., 2014. A Cenozoic-style
516 scenario for the end-Ordovician glaciation. Nature Communications 5, paper number
517 4485, doi: 10.1038/ncomms5485.

518 Gürsu, S., Mueller, P.A., Sunkari, E.D., Möller, A., Köksal, S., Kamenov, G.D., and
519 Göncüoğlu, M.C., 2018. Nd, Pb, Hf isotope characteristics and provenance of glacial
520 granitic pebbles from Late Ordovician diamictites in the Taurides, S Turkey.
521 Gondwana Research 54, 205–216.

522 Henderson, B.J., Collins, W.J., Murphy, J.B., Gutierrez-Alonso, G., and Hand, M., 2015.
523 Gondwanan basement terranes of the Variscan–Appalachian orogen: Baltican,
524 Saharan and West African hafnium isotopic fingerprints. Tectonophysics 681, 278–
525 304.

526 Hoepffner, C., Soulaimani, A., and Piqué, A., 2005. The Moroccan Hercynides. Journal of
527 African Earth Sciences 43, 144–165.

528 Hofmann, M., Linnemann, U., Hoffmann, K.H., Germs, G., Gerdes, A., Marko, L., Eckelmann,
529 K., Gärtner A., and Krause, R., 2015. The four Neoproterozoic glaciations of southern
530 Namibia and their detrital zircon record: The fingerprints of four crustal growth
531 events during two supercontinent cycles. Precambrian Research 259, 176–188.

532 Huang, J., Feng, L., Lu, D., Zhang, Q., Sun, T., Chu, X. 2014. Multiple climate cooling prior to
533 Sturtian glaciations: Evidence from chemical index of alteration of sediments in South
534 China. Scientific Reports 4, 6868.

535 Jackson, S.E., Pearson, N.J., Griffin, W.L., and Belousova, E.A., 2004. The application of
536 laser ablation-inductively coupled plasma-mass spectrometry to in situ U–Pb zircon
537 geochronology. Chemical Geology 211, 47-69.

538 Jackson, S., 2008. Lamtrace data reduction software for LA-ICP-MS. In: Sylvester, P. J.
539 (Ed.), Laser Ablation-ICP-MS in the Earth Sciences: Current Practices and Outstanding
540 Issues, pp. 305–307 Mineralogical Association of Canada.

541 Jaffey, A.H., Flynn, K.F., Glendenin, L.E., Bentley, W.C., Essling, A.M., 1971. Precision
542 measurements of half-lives and specific activities of ^{235}U and ^{238}U. Physical Reviews C
543 4, 1889-1906.

544 Le Heron, D., 2007. Late Ordovician glacial record of the Anti-Atlas, Morocco.
545 Sedimentary Geology 201, 93–110.

546 Le Heron, D., Ghienne, J.-F., El Houicha, M., Khoukhi, Y., and Rubino, J.-L, 2007. Maximum
547 extent of ice sheets in Morocco during the Late Ordovician glaciation.
548 Palaeogeography Palaeoclimatology Palaeoecology 245, 200–226.

549 Le Heron, D.P., Khoukhi, Y., Paris, F., Ghienne, J.-F. and Le Herissé, A., 2008 ; Black shale,
550 grey shale, fossils and glaciers: Anatomy of the Upper Ordovician–Silurian succession
551 in the Tazzeka Massif of eastern Morocco. Gondwana Research 14, 483–496.

552 Le Heron, D.P., and Craig, J., 2008. First-order reconstructions of a Late Ordovician
553 Saharan ice sheet. Journal of Geological Society 165, 19–29.

554 Letsch D., El Houicha M., von Quadt A., and Winkler, W.A., 2018. A missing link in the
555 peri-Gondwanan terrane collage: the Precambrian basement of the Moroccan Meseta
556 and its Lower Paleozoic cover. Canadian Journal of Earth Sciences 55, 33–51.

557 Linnemann, U., Ouzegane, K., Drareni, A., Hofmann, M., Becker, S., Gärtner, A., and
558 Sagawe, A., 2011. Sands of West Gondwana: An archive of secular magmatism and
559 plate interactions — A case study from the Cambro-Ordovician section of the Tassili
560 Ouan Ahaggar (Algerian Sahara) using U–Pb–LA-ICPMS detrital zircon ages. Lithos
561 123, 188–203.

562 Loi, A., Ghienne, J.-F., Dabard, M.P. , Paris, F. , Botquelen, A., Christ, N., Elaouad-Debbaj, Z.,
563 Gorini, A., Vidal, M., Videt, B. and Destombes, J., 2010. The Late Ordovician glacio-
564 eustatic record from a high-latitude storm-dominated shelf succession: The Bou
565 Ingarf section (Anti-Atlas, Southern Morocco). Paleogeography Paleoclimatology
566 Paleoecology 296, 332–358.

567 Longerich, H. P., Jackson, S. E., and Gunther, D., 1996. Inter-laboratory note. Laser
568 ablation inductively coupled plasma mass spectrometric transient signal data
569 acquisition and analyte concentration calculation. Journal of Analytical Atomic
570 Spectrometry 11, 899–904.

571 Ludwig, K.R., 2012. User's manual for Isoplot 3.75 : A geochronological toolkit for
572 Microsoft Excel. Berkley Geochronology Center Special Publication No.5.

573 Martinez-Catalan, J.R., Hacar Rodriguez, P.P., Villar Alonso, P., Perez-Estaun, A. and
574 Gonzalez Lodeiro, F., 1992. Lower Paleozoic extensional tectonics in the limit
575 between the West Asturian-Leonese and Central Iberian Zones of the Variscan Fold-
576 Belt in NW Spain. Geologische Rundschau 81/2, 545–560.

577 McLennan, S. M., Hemming, S., McDaniel, D. K., and Hanson, G. N., 1993. Geochemical
578 approaches to sedimentation, provenance, and tectonics. In: Johnsson, M. l. & Basu, A.
579 (Eds.), Processes Controlling the Composition of Clastic Sediments, pp. 21-40
580 Geological Society of America, Special Paper.

581 McLennan, S. M., Bock, B., Hemming, S., Hurowitz, J. A., Lev, S. M., and McDaniel , D. K.,
582 2003. The role of provenance and sedimentary processes in the geochemistry of
583 sedimentary rocks. In Lentz, D. R. (ed.): Geochemistry of Sediments and Sedimentary
584 Rocks: Evolutionary Considerations to Mineral Deposit-Fanning Environments, pp. 7–
585 38 Geological Association of Canada, GeoTexl 4.

586 Marzoli, A., Davies, J.H.F.L., Youbi, N., Merle, R., Dal Corso, J., Dunkley, D.J., Fioretti, A.M.,
587 Bellieni, G., Medina, F., Wotzlaw, J.-F., McHone, G., Font, E. and Bensalah, M.K., 2017.
588 Proterozoic to Mesozoic evolution of North-West Africa and Peri-Gondwana
589 microplates: detrital zircon ages from Morocco and Canada. Lithos 278-281, 229–239.

590 Meinhold, G., Morton, A.C., Avigad D., 2013. New insights into peri-Gondwana
591 paleogeography and the Gondwana super-fan system from detrital zircon U–Pb ages.
592 Gondwana Research 23, 661–665.

593 Michard, A., Soulaimani, A., Hoepffner, C., Ouanaimi, H., Baidder, L., Rjimati, E.C., and
594 Saddiqi, O., 2010. The south-western branch of the Variscan belt: Evidence from
595 Morocco. Tectonophysics 492, 1–24.

596 Nesbitt, H., W., 2003. Petrogenesis of siliciclastic sediments and sedimentary rocks. In:
597 Lentz, D. R. (Ed.): Geochemistry of Sediments and Sedimentary Rocks: Evolutionary
598 Considerations to Mineral Deposit-Forming Environments, pp. 39–51 Geological
599 Association of Canada, GeoText 4

600 Nesbitt, H. W., and Young, G. M., 1982. Early Proterozoic climates and plate motions
601 inferred from major element chemistry of lutites. Nature 299, 715–717.

602 Ouanaimi H., Soulaimani A., Hoepffner C., Michard A., and Baidder L., 2016. The Atlas-
603 Meseta Red Beds basin (Morocco) and the Lower Ordovician rifting of NW-
604 Gondwana. Bulletin de la Société Géologique de France 187, 155–168.

605 Paton, C., J. D. Woodhead, J. C. Hellstrom, J. M. Hergt, A. Greig, and R. Maas, 2010.
606 Improved laser ablation U-Pb zircon geochronology through robust downhole
607 fractionation correction. Geochemistry Geophysics. Geosystems 11, paper number
608 Q0AA06, doi:10.1029/2009GC002618.

609 Pastor-Galán, D., Gutiérrez-Alonso, G., Murphy, J.B., Fernández-Suárez, J., Hofmann, M.,
610 and Linnemann, U., 2013. Provenance analysis of the Paleozoic sequences of the
611 northern Gondwana margin in NW Iberia: passive margin to Variscan collision and
612 orocline development. Gondwana Research 23, 1089–1103.

613 Pérez-Càceres, I., Poyatos, D.M., Simancas, J.F., and Azor, A., 2017. Testing the Avalonian
614 affinity of the South Portuguese Zone and the Neoproterozoic evolution of SW Iberia
615 through detrital zircon populations. Gondwana Research 42, 177–192.

616 Pistis, M., Loi, A. and Dabard, M.-P, 2016. Influence of relative sea-level variations on the
617 genesis of palaeoplacers, the examples of Sarrabus (Sardinia, Italy) and the
618 Armorican Massif (western France). Comptes Rendus Geosciences 348, 150–157.

619 Pohl, A., Donnadieu, Y., Le Hir, G., Ladant, J.B., Dumas, C., Alvarez-Solas, J. and
620 Vandenbroucke, T.R.A., 2016. Glacial onset predated Late Ordovician climate cooling,
621 Paleoceanography 31, 800–821.

622 Pouclet, A., Ouazzani H., and Fekkak A., 2008. The Cambrian volcano-sedimentary
623 formations of the westernmost High Atlas (Morocco): Their place in the geodynamic
624 evolution of the West African Palaeo-Gondwana northern margin. In: Ennih N.,
625 Liégeois J.-P. (Eds): The Boundaries of the West African Craton, Geological Society
626 London, Spec. Publ 297, 303–327.

627 Pratt, J.R., Barbeau, D.L.Jr., Garver, J.I., Emran, A., and Izykowski, T.M., 2015. Detrital
628 zircon geochronology of Mesozoic sediments in the Rif and Middle Atlas Belts of
629 Morocco: Provenance constraints and refinement of the West African signature.
630 Journal of Geology 123, 177–200.

631 Ravier, E., Buoncristiani, J. F., Menzies, J., Guiraud, M., Clerc, S., and Portier, E., 2015. Does
632 porewater or meltwater control tunnel valley genesis? Case studies from the

633 Hirnantian of Morocco. Palaeogeography Palaeoclimatology Palaeoecology 418, 359–
634 376.

635 Razin, P., Baudin, T., Chevremont, P., Andies, D., Youbi, N., Hoepffner, C., Thieblemont, D.,
636 and Chichani, E.-M., 2002. Carte Géologique 1/50000, Jebel Kharrou. Notes et
637 Mémoires du Service Géologique du Maroc 436 bis, 104 pp.

638 Rognon, P., Biju-Duval, B., and De Charpal, O., 1972. Modelés glaciaires dans l'Ordovicien
639 supérieur saharien: phases d'érosion et glaciotectonique sur la bordure nord des
640 Eglab. Revue de Géographie Physique et Dynamique 14, 507–528.

641 Roser, B.P. and Korsch, R.J., 1988. Provenance signatures of Sandstone-mudstone suites
642 determined using discriminant function analysis of major-elment data. Chemical
643 Geology 67, 119–139.

644 Shaw, J., Gutiérrez-Alonso, G., Johnston, S. T. and Galán, D. P. 2014. Provenance
645 variability along the Early Ordovician north Gondwana margin: Paleogeographic and
646 tectonic implications of U-Pb detrital zircon ages from the Armorican Quartzite of the
647 Iberian Variscan belt. Geological Society of America Bulletin 126, 702–719.

648 Sláma, J., Košler, J., Condon, D.J., Crowley, J.L., Gerdes, A., Hanchar, J.M., Horstwood,
649 M.S.A., Morris, G.A., Nasdala, L., Norberg, N., Schaltegger, U., Schoene, N., Tubrett, M.N.,
650 and Whitehouse, M.J., 2008. Plešovice zircon - a new natural reference material for U–
651 Pb and Hf isotopic microanalysis. Chemical Geology 249, 1–35.

652 Tahiri, A., Montero P., El Hadi H., Martínez Poyatos D., Azor A., Bea F., Simancas J.F., and
653 González Lodeiro, F., 2010. Geochronological data on the Rabat – Tiflet granitoids:
654 Their bearing on the tectonics of the Moroccan Variscides. Journal of African Earth
655 Sciences 57, 1–13.

656 Taylor, S.R., and McLennan, S.M., 1985. The continental crust: Its composition and
657 evolution. Blackwell Scientific Pub., Palo Alto, CA, United States.

658 Wedepohl, H.K., 1995. The composition of continental crust. Geochimica Et
659 Cosmochimica Acta 59, 1217–1232.

660 Wiedenbeck, M., Alle, P., Corfu, F., Griffin, W.L., Meier, M., Oberli, F., von Quadt, A.,
661 Roddick, J.C., and Spiegel, W., 1995. Three natural zircon standards for U–Th–Pb, Lu–
662 Hf, trace element and REE analyses. Geostandards Newsletter 19, 1–23.

663 Yan, D., Chen, D., Wang, Q., and Wang, J., 2010. Large-scale climatic fluctuations in the
664 latest Ordovician on the Yangtze block, south China. Geology 38, 599–601.

665 Young, M.G., Minter, W.E.L., and Theron, J.N., 2004. Geochemistry and palaeogeography
666 of upper Ordovician glaciogenic sedimentary rocks in the Table Mountain Group,
667 South Africa. Paleogeography Paleoclimatology Paleoecology 214, 323–345.